An Efficient Algorithm for the Three-Dimensional Analysis of Passive Microstrip Components and Discontinuities for Microwave and Millimeter-Wave Integrated Circuits

Achim Hill and Vijai K. Tripathi, *Senior Member, IEEE*

Abstract —**A numerical technique for the full-wave analysis of shielded, passive microstrip components on a two-layer substrate is presented. The distinct feature of the technique is a novel, efficient formulation for establishing the system matrix in the moment method procedure which allows the derivation of the elements of any large matrix by a linear combination of elements in a precomputed index table. The table is obtained from a two-dimensional discrete fast Fourier transform. In the moment method procedure, the two-dimensional surface current is represented by locally defined rooftop functions. The effect of the resonant modes associated with the metallic enclosure on the numerical procedure is examined. In order to demonstrate the features and the accuracy of the technique, numerical results for microstrip open end and for a right-angle bend with and without the compensated corner are computed by using the resonant technique and are compared with other published computational and experimental data.**

I. Introduction

A considerable amount of work has been done in recent years on the frequency-dependent characterization and modeling of microstrip components and discontinuities, resulting in several useful numerical techniques [1]. These include solutions based on waveguide and two-dimensional cavity models, use of the method of lines, finite difference and finite element techniques, and the solution based on an integral equation formulation in real space and the Fourier transform domain [1]–[31]. All the accurate methods are, in general, computationally intensive; devising techniques to improve the efficiency of various methods continues to be a challenging task.

The integral equation formulation in real space and the spectral domain has become a promising technique for the analysis and simulation of components and discontinuities in microwave and millimeter-wave circuits. The simulation of passive (M)MIC structures can be classified into three categories, namely open, shielded, and partly shielded configurations. Each shielding type requires a somewhat different numerical treatment. Efficient computational methods have been derived for the open [21] and partly shielded structures [23]. However, the shielded configuration still requires intensive computational treatment. The insufficient development of full-wave simulators which accurately incorporate housing effects has also been pointed out recently by Jansen and Wiemer [25].

In this paper a technique which allows for an efficient numerical treatment of the shielded circuit structure is presented. It leads to reasonable computation times for the analysis of 3-D microstrip structures for the case when 2-D locally defined surface currents are employed in the moment method. The analysis represents an extension of the previous work reported by Jansen [7], Koster [8], Rautio and Harrington [12], [13] and Dunleavy and Katehi [27], [28].

Manuscript received October 23, 1989; revised July 24, 1990.

A. Hill was with the Department of Electrical and Computer Engineering, Oregon State University, Corvallis, OR 97331. He is now with Compact Software Inc., Paterson, NJ 07504.

V. K. Tripathi is with the Department of Electrical and Computer Engineering, Oregon State University, Corvallis, OR 97331.

IEEE Log Number 9040562.

II. Matrix Equation Formulation

Consider the boxed structure shown in Fig. 1. The source-free medium consists of three homogeneous, isotropic dielectric layers and is bounded by a box of perfectly conducting metal. Each layer r $(r = 1,2,3)$ of thickness H_r is characterized by its relative dielectric constant ϵ_r. The box extends from $x = 0$ to $x = a$, $y = 0$ to $y = b$ with bottom and cover plates at $z = 0$ and $z = c$. The microstrip metallization of zero thickness and infinite conductivity is located at the interface.

The tangential electric field components on the interface (E_x, E_y) are expressed in terms of surface currents (J_x, J_y):

$$\begin{aligned} E_x = {} & \sum_m \sum_n F_{mn} XY_{mn} \int J_x(x', y') \cos k_{xm} x' \sin k_{yn} y' dx' dy' \\ & \cdot \cos k_{xm} x \sin k_{yn} y \\ & + \sum_m \sum_n F_{mn} RZ_{mn} \int J_y(x', y') \sin k_{xm} x' \cos k_{yn} y' dx' dy' \\ & \cdot \cos k_{xm} x \sin k_{yn} y \\ E_y = {} & \sum_m \sum_n F_{mn} RZ_{mn} \int J_x(x', y') \cos k_{xm} x' \sin k_{yn} y' dx' dy' \\ & \cdot \sin k_{xm} x \cos k_{yn} y \\ & + \sum_m \sum_n F_{mn} YX_{mn} \int J_y(x', y') \sin k_{xm} x' \cos k_{yn} y' dx' dy' \\ & \cdot \sin k_{xm} x \cos k_{yn} y. \end{aligned} \tag{1}$$

0018-9480/91/0100-0083$01.00 ©1991 IEEE

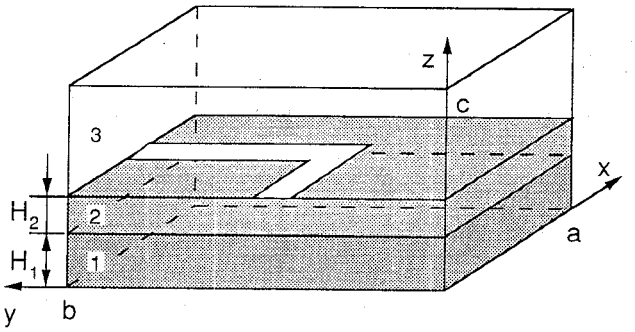

Fig. 1. Microstrip discontinuity in shielded box.

The expressions $F_{mn}XY_{mn}$, $F_{mn}R_{mn}$, and $F_{mn}YX_{mn}$ represent the components of the spectral-domain Green's dyadic. These have been derived by Jansen and Koster [7], [8] and they are summarized in the Appendix for convenience. The discrete spectral variables in the above equation are given by $k_{xm} = m\pi/a$ and $k_{yn} = n\pi/b$.

Equation (1), a Fredholm integral equation of the first kind, maps the surface current into an electric field on the interface. Following the moment method procedure, the current is expanded into basis functions and substituted in (1). In a subsequent step (1) is tested with suitable functions which in the present case were chosen to be identical to the basis functions leading to a Galerkin implementation of the method. The present method employs rooftop functions as the basis elements [13], [15]–[17]. Fig. 2 shows the discretization of the metallized surface with discretization Δx and Δy in the x and y directions, respectively. The center of x-directed currents is marked with a cross, and the center of y-directed currents is marked with a circle. Note that the x- and y-directed currents are offset by $(\Delta x/2, \Delta y/2)$ in order to ensure edge conditions and generate correct results. A detailed discussion for the current offset can be found in [12]. The total current is approximated by

$$J = \sum_k a_{xk} J_{xx}(x, x_k) J_{xy}(y, y_k) + \sum_i a_{yi} J_{yx}(x, x_i), J_{yy}(y, y_i) \tag{2}$$

where

$$J_{uu}(u, u_k) = \begin{cases} \dfrac{u - u_k}{\Delta u} + 1, & u_k - \Delta u < u < u_k \\ \dfrac{u_k - u}{\Delta u} + 1, & u_k < u < u_k + \Delta u \\ 0, & \text{otherwise} \end{cases} \tag{3}$$

with $u = x$ or y and

$$J_{uv}(v, v_k) = \begin{cases} 1, & v_k - \Delta v/2 < v < v_k + \Delta v/2 \\ 0, & \text{otherwise} \end{cases} \tag{4}$$

with $uv = xy$ or yx.

After applying the testing procedure, the linear system of equations can be summarized as follows:

$$\begin{bmatrix} V_x \\ V_y \end{bmatrix} = \begin{bmatrix} P_{xx} & P_{xy} \\ P_{yx} & P_{yy} \end{bmatrix} \begin{bmatrix} A_x \\ A_y \end{bmatrix}. \tag{5}$$

The left-hand side represents the scalar product of the electric field and a testing function at the ith subsection. These vanish on the metal except for subsections where sources are defined. The P matrix contains the testing products and the Green's dyadic of the associated boundary value problem. Vector A is formed by the expansion coefficients for current as given in (2), i.e., $A_{xi} = a_{xi}$ and $A_{yi} = a_{yi}$. In the above equation,

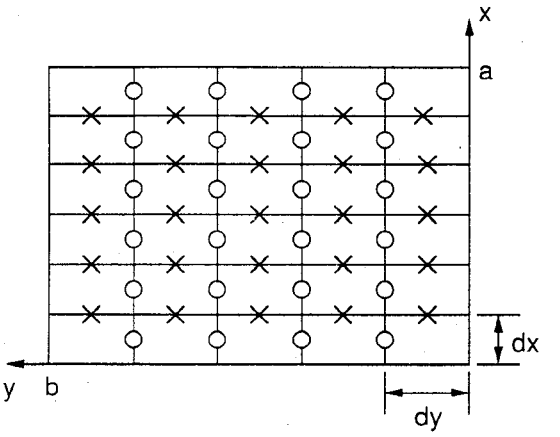

Fig. 2. Discretization of conductor surface. Crosses represent center of x-directed current; circles represent centers of y-directed currents.

$$V_{xi} = \int\int E_x J_{xi}\, dx\, dy$$

$$V_{yi} = \int\int E_y J_{yi}\, dx\, dy \tag{6}$$

$$P_{xx}^{ij} = \sum_m \sum_n G_{mn}^{xx} \cos k_{xm} x_{jx} \sin k_{yn} y_{jx} \cos k_{xm} x_{ix} \sin k_{yn} y_{ix}$$

$$P_{xy}^{ij} = \sum_m \sum_n G_{mn}^{xy} \sin k_{xm} x_{jy} \cos k_{yn} y_{jy} \cos k_{xm} x_{ix} \sin k_{yn} y_{ix}$$

$$P_{yx}^{ij} = \sum_m \sum_n G_{mn}^{yx} \cos k_{xm} x_{jx} \sin k_{yn} y_{jx} \sin k_{xm} x_{iy} \cos k_{yn} y_{iy}$$

$$P_{yy}^{ij} = \sum_m \sum_n G_{mn}^{yy} \sin k_{xm} x_{jy} \cos k_{yn} y_{jy} \sin k_{xm} x_{iy} \cos k_{yn} y_{iy} \tag{7}$$

and

$$\begin{aligned} G_{mn}^{xx} &= F_{mn} XY_{mn} G_t^2(\Delta x) G_r^2(\Delta y) \\ G_{mn}^{xy} &= F_{mn} R_{mn} G_t(\Delta y) G_r(\Delta x) G_t(\Delta x) G_r(\Delta y) \\ G_{mn}^{yx} &= F_{mn} R_{mn} G_t(\Delta x) G_r(\Delta y) G_t(\Delta y) G_r(\Delta x) \\ G_{mn}^{yy} &= F_{mn} YX_{mn} G_t^2(\Delta y) G_r^2(\Delta x) \end{aligned} \tag{8}$$

where

$$G_t(\Delta u) = \begin{cases} \dfrac{2}{\Delta u k_u^2}(1 - \cos(k_u \Delta u)), & k_u \neq 0 \\ \Delta u, & k_u = 0 \end{cases} \tag{9}$$

$$G_r(\Delta u) = \begin{cases} \dfrac{2}{k_u}(\sin(k_u \Delta u/2), & k_u \neq 0 \\ 0, & k_u = 0. \end{cases} \tag{10}$$

III. Enhanced Algorithm

The evaluation of the elements P^{ij} of the moment matrix is time consuming owing to the two-dimensional summation and the repeated computation of the Green's dyadic with associated harmonic functions, and the time requirement for the solution of the linear system (9) is negligible compared with the formation of the matrix.

In addition to the possible use of fast Fourier transform (FFT), efficiency considerations for the summation procedure in (7) have already been discussed by Rautio [12], where the periodicity of the harmonic functions was used to develop a summation scheme which avoids the periodic evaluation of the trigonometric functions. The present approach makes use of two techniques which lead to drastic reductions of computation times. The first technique employs customized 2-D FFT routines to compute the index tables, and the second constitutes the application of specialized indexing routines which allow the derivation of all elements of the moment matrix by a simple linear combination of elements of the index tables. This second technique completely eliminates the $IEX \cdot (IEX-1)/2$ operations for the formation of the moment matrix, where IEX is the total number of expansion functions.

In order to employ FFT subroutines the representation of the moment matrix has to be transformed into a suitable form. In addition, the interface is uniformly discretized in x and y directions such that

$$\begin{aligned} x_{ix} &= p_{ix}\Delta x, & p_{ix} &= 0,1,\cdots,M \\ y_{iy} &= s_{iy}\Delta y, & s_{iy} &= 0,1,\cdots,N \\ x_{iy} &= \left(p_{iy}+\tfrac{1}{2}\right)\Delta x, & p_{iy} &= 0,1,\cdots,M-1 \\ y_{ix} &= \left(s_{ix}+\tfrac{1}{2}\right)\Delta y, & s_{ix} &= 0,1,\cdots,N-1. \end{aligned} \quad (11)$$

Since the respective operator of the Fredholm integral equation (1) is self-adjoint, the moment matrix is symmetric and P_{yx}, which is equal to P_{xy}, is no longer considered in the numerical treatment. After using trigonometric identities and substituting (11) into (7), the moment matrix P can be rewritten as

$$\begin{aligned} P_{xx}^{ij} = {} & f_{xx}(p_{jx}-p_{ix},s_{jx}-s_{ix}) - f_{xx}(p_{jx}-p_{ix},s_{jx}+s_{ix}) \\ & + f_{xx}(p_{jx}+p_{ix},s_{jx}-s_{ix}) - f_{xx}(p_{jx}+p_{ix},s_{jx}+s_{ix}) \end{aligned} \quad (12)$$

$$\begin{aligned} P_{xy}^{ij} = {} & f_{xy}(p_{jy}+p_{ix},s_{jy}+s_{ix}) - f_{xy}(p_{jy}+p_{ix},s_{jy}+s_{ix}) \\ & + f_{xy}(p_{jy}-p_{ix},s_{jy}+s_{ix}) - f_{xy}(p_{jy}-p_{ix},s_{jy}-s_{ix}) \end{aligned} \quad (13)$$

$$\begin{aligned} P_{yy}^{ij} = {} & f_{yy}(p_{jy}-p_{iy},s_{jy}-s_{iy}) + f_{yy}(p_{jy}-p_{iy},s_{jy}+s_{iy}) \\ & - f_{yy}(p_{jy}+p_{iy},s_{jy}-s_{iy}) - f_{yy}(p_{jy}+p_{iy},s_{jy}+s_{iy}) \end{aligned} \quad (14)$$

with

$$\begin{aligned} f_{xx}(u,v) &= \sum_m \sum_n G_{mn}^{xx} \cos\frac{m\pi u}{M}\cos\frac{n\pi v}{N} \\ f_{xy}(u,v) &= \sum_m \sum_n G_{mn}^{xy} \sin\frac{m\pi(u+1/2)}{M}\sin\frac{n\pi(v+1/2)}{N} \\ f_{yy}(u,v) &= \sum_m \sum_n G_{mn}^{yy} \cos\frac{m\pi u}{M}\cos\frac{n\pi v}{N}. \end{aligned} \quad (15)$$

The expressions for P^{ij}, (12)–(14), are now in a form which is suited for the application of 2-D discrete FFT's. If we were to compute each element of the moment matrix by using the FFT algorithm, we would require $IT = IEX*(IEX-1)/2$ evaluations for a matrix with dimensions IEX, e.g. IT = 4485 if IEX = 300. The technique presented here allows us to reduce the IT evaluations to IT = three evaluations for any matrix size. The elements P^{ij} are obtained from a linear combination of components of the FFT's with respect to the transform variable, as will be outlined in the following. Instead of computing (12)–(14) for each $P_{xx}^{ij}, P_{xy}^{ij}, P_{yy}^{ij}$, only three FFTs are computed and stored in suitable arrays:

$$P_{xx}(u,v) = f_{xx}(u,v), \qquad u=0,\cdots,M;\ v=0,\cdots,N \quad (16)$$

$$P_{xy}(u,v) = f_{xy}(u,v), \qquad u=0,\cdots,M-1;\quad v=0,\cdots,N-1 \quad (17)$$

$$P_{yy}(u,v) = f_{yy}(u,v), \qquad u=0,\cdots,M;\ v=0,\cdots,N. \quad (18)$$

The elements of the moment matrix are then derived from a linear combination of (16)–(18), as implied in (12)–(14) under consideration of the periodicy of the trigonometric functions.

The double infinite summations have to be truncated at a suitable bound such that a certain convergence criterion is fulfilled. This upper bound can exceed the period of the respective FFT's. In other words, the sampling ratio, defined as the number of spatial frequency samples per discretization length, is larger than unity. To circumvent this problem, the functions G_{mn} in (20) are presampled at periodic intervals to form a summation which is then submitted to the FFT routines. The idea of such a first-stage summation has been used before, by Rautio [12]; however, the implementation was different. As a consequence of the first-stage summation scheme, each of the three FFT's in (21)–(23) is split into four FFT's, which yields a total number of 12 FFT's for the evaluation of a moment matrix. To incorporate an arbitrary number of spatial frequencies in the FFT algorithm, the three basic FFT formulations given in (16)–(18) are decomposed as follows.

$$\begin{aligned} &\sum_m \sum_n G_{mn}^{xx} \cos\frac{m\pi p}{M}\cos\frac{n\pi s}{N} \\ &\quad = \sum_m \sum_n G_{mn}^{xxee} \cos\frac{m\pi p}{M}\cos\frac{n\pi s}{N} \\ &\qquad + (-1)^s \sum_m \sum_n G_{mn}^{xxeo} \cos\frac{m\pi p}{M}\cos\frac{n\pi s}{N} \\ &\qquad + (-1)^p \sum_m \sum_n G_{mn}^{xxoe} \cos\frac{m\pi p}{M}\cos\frac{n\pi s}{N} \\ &\qquad + (-1)^{(s+p)} \sum_m \sum_n G_{mn}^{xxoo} \cos\frac{m\pi p}{M}\cos\frac{n\pi s}{N} \end{aligned} \quad (19)$$

$$\begin{aligned} &\sum_m \sum_n G_{mn}^{xy} \sin\frac{m\pi(p+1/2)}{M}\sin\frac{n\pi(s+1/2)}{N} \\ &\quad = \sum_m \sum_n G_{mn}^{xyee} \sin\frac{m\pi(p+1/2)}{M}\sin\frac{n\pi(s+1/2)}{N} \\ &\qquad + (-1)^s \sum_m \sum_n G_{mn}^{xyeo} \sin\frac{m\pi(p+1/2)}{M} \\ &\qquad \cdot \cos\frac{n\pi(s+1/2)}{N} \\ &\qquad + (-1)^p \sum_m \sum_n G_{mn}^{xyoe} \cos\frac{m\pi(p+1/2)}{M} \\ &\qquad \cdot \sin\frac{n\pi(s+1/2)}{N} \\ &\qquad + (-1)^{(s+p)} \sum_m \sum_n G_{mn}^{xyoo} \cos\frac{m\pi(p+1/2)}{M} \\ &\qquad \cdot \cos\frac{n\pi(s+1/2)}{N}. \end{aligned} \quad (20)$$

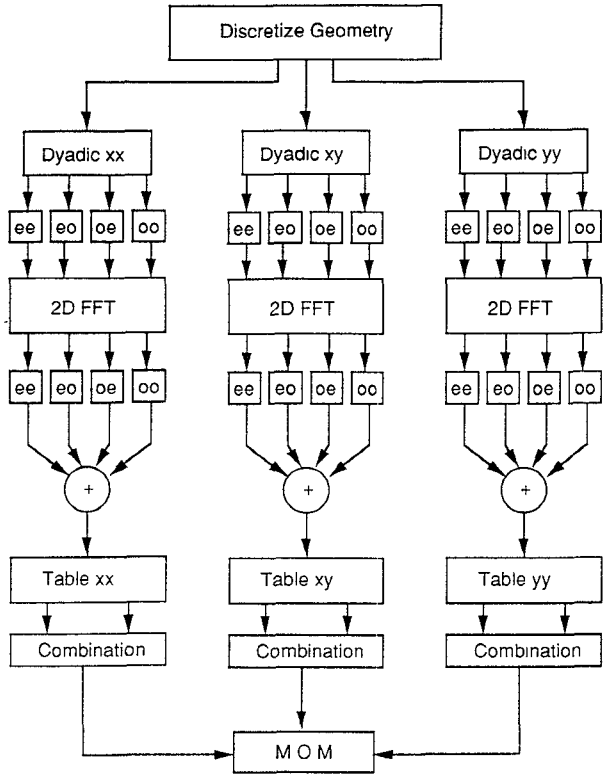

Fig. 3. Enhanced algorithm for establishing the moment matrix (MOM).

The quantity

$$\sum_m \sum_n G_{mn}^{yy} \cos \frac{m\pi p}{M} \cos \frac{n\pi s}{N}$$

is identical to (24) with G_{mn}^{xx} replaced by G_{mn}^{yy}. The abbreviations in (24) and (25) are defined as follows:

$$G_{mn}^{xxpq} = \sum_{i_p} \sum_{j_q} (m + i_p M, n + j_q N)$$

$$G_{mn}^{yypq} = \sum_{i_p} \sum_{j_q} (m + i_p M, n + j_q N)$$

$$G_{mn}^{xypq} = \sum_{i_p} \sum_{j_q} G^{xy}(m + i_p M, n + j_q N)(-1)^{(i_p/2 + j_q/2)} \quad (21)$$

with $p = e$ or O and $q = e$ or O and $i_e, j_e = 0, 2, 4, \cdots$; $i_o, j_o = 1, 3, 5, \cdots$. The formation of the moment matrix is summarized in Fig. 3. After discretizing the geometry, each Green's dyadic together with the associated spectral representation of the basis functions is presampled as suggested in (26). Next, 2-D FFT's are applied as outlined in (16) through (18). Results of the FFT's are then stored to form index tables. Now the moment matrix of any geometry on the discretized interface can be built by a suitable linear combination of the elements of the three index tables as implied in (12) through (14).

IV. Numerical Results

The algorithm described above is applicable to both deterministic and eigenvalue problems [8], [12], [27]. The deterministic procedure as discussed in [12] and [27] allows for the derivation of port impedances for given excitations at the terminal ports. These impedance values are then used for the determination of the network matrix. The eigenvalue formulation requires the evaluation of the resonance frequency of the microstrip structure in the shielding box, from which discontinuity parameters are extracted as shown in [7], [8], and [32]. We have used the deterministic approach for the first example only and the eigenvalue computation approach for all the subsequent examples.

As an initial confidence test for the presented technique, the input impedance of a microstrip stub was computed and compared with results obtained by Rautio and Harrington [13]. The box was 4 cm long, 2 cm wide, and 5 cm high. The strip line was 1 cm wide and 2.81 cm long and was deposited on a 1-cm-thick substrate with a relative dielectric constant of 10. The results are shown in Fig. 4 and the agreement is obvious.

The open end discontinuity of a microstrip line can be characterized by an effective length extension, l_{eff}, or an equivalent terminating capacitance which accounts for the fringing fields at the open end. Dynamic simulation of the open end effect in a shielded environment have recently been developed by Jansen and Koster [30] and Dunleavy and Katehi [26], and these are included for comparison in Fig. 5. The shielding geometry and strip dimensions were chosen to be identical to those used in [26]. The box was 7.747 mm wide and 5.08 mm high. The frequency behavior of the effective length computed in this work behaves in the same manner as described by Koster [8]. For low frequencies the length decreases then passes through a minimum and increases for higher frequencies. The box used in the presented analysis exhibits a resonance around 24 GHz for the specified dimensions, which explains the deviation of the effective length at this point from the results obtained in [26] and [29].

The S parameters for typical right-angle-bend geometries having various W/H ratios are shown in Fig. 6 for an alumina substrate of height 0.635 mm. All bends are analyzed in a square box of 12.7 mm side length and 3.81 mm height. For the nominal 50 Ω line ($W/H \simeq 1$) S-parameter simulations are compared with design formulas from Kirschning *et al.* [30], which were derived from measurements in the frequency range between 2 and 14 GHz for an open structure. The deviation in magnitude of S_{11} is within 3% for the frequency range up to 14 GHz. However, larger differences are observed for the phase beyond 4 GHz. These differences are attributed to the effect of the shielding box used in these computations.

Next, a bend is simulated in the frequency range between 50 and 120 GHz to demonstrate the effect of parasitic box resonances. The bend of 100 μm width is deposited on a 100 μm GaAs substrate with a 5 μm oxide layer. The box dimensions were $a = 1.9$ mm and $c = 1.05$ mm. Fig. 7 shows the associated S parameters. To show the effect of box resonances, the height of the box is reduced to $c = 200$ μm. The oxide layer is removed in this example. Investigations of the first LSM_{10} parametric waveguide mode predict a resonance in the vicinity of 80 GHz, which is verified by the S-parameter computation shown in Fig. 8.

As a last example, the S parameters of a right-angle bend are compared for a compensated corner. The compensation is obtained by cutting out a square at the corner of the bend. The form of the compensation is shown in the inset of

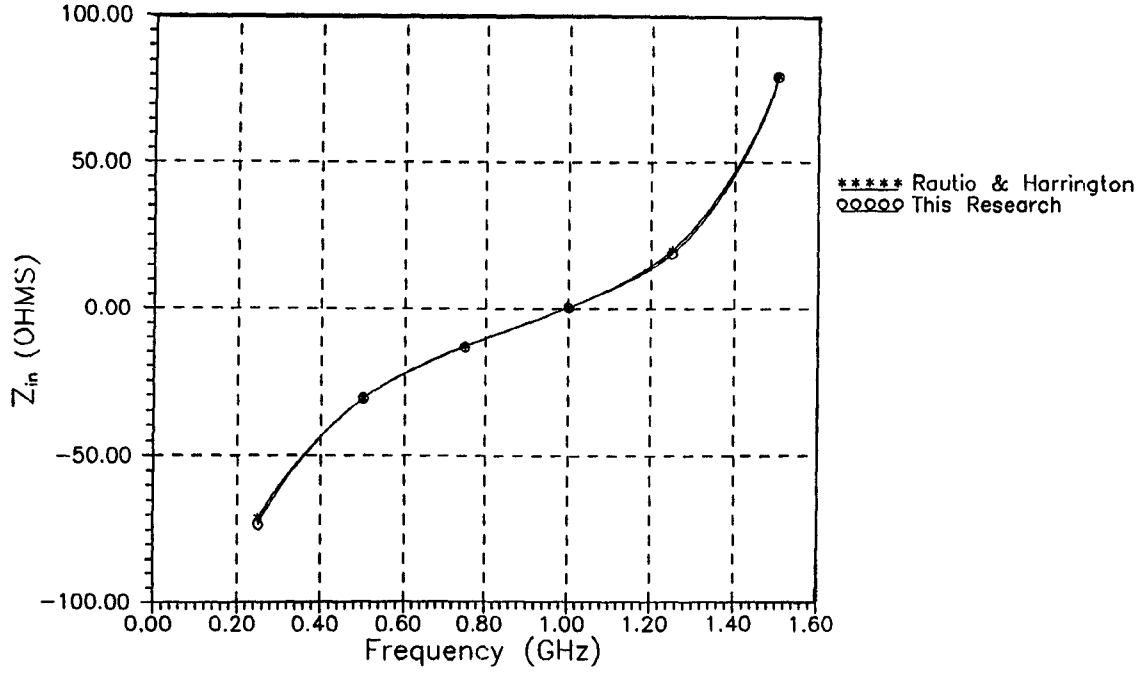

Fig. 4. Stub input impedance ($a = 2$ cm, $b = 4$ cm, $c = 5$ cm, $H_1 = 1$ cm, $\epsilon_1 = 10$).

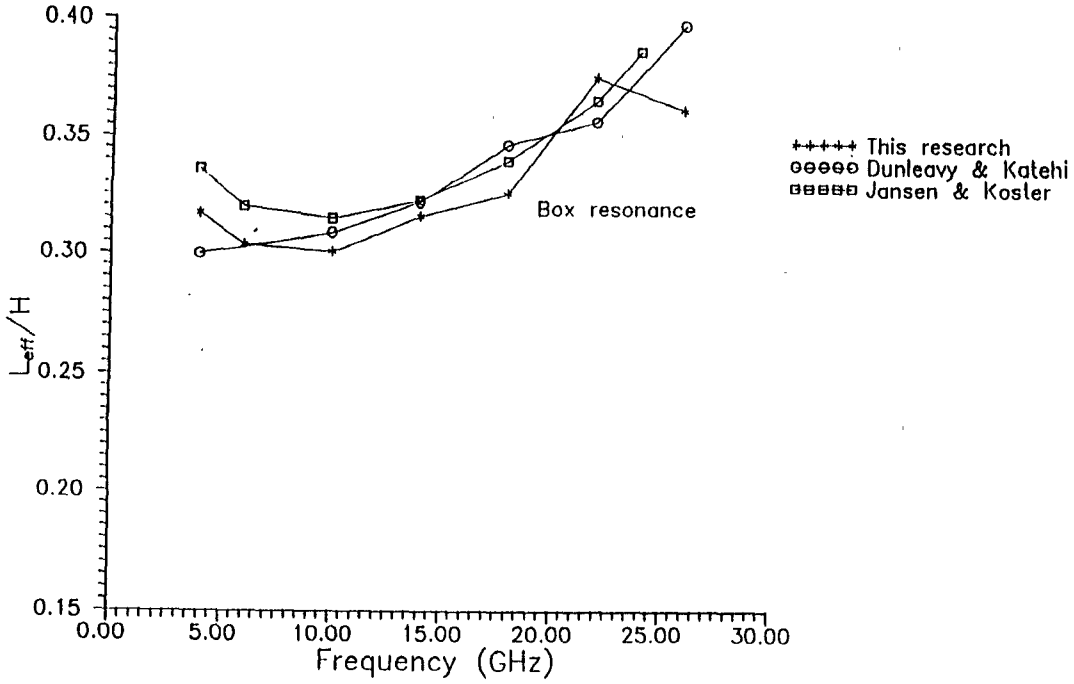

Fig. 5. Effective length of open microstrip end ($a = 7.747$ mm, $c = 5.08$ mm, $H_1 = 0.635$ mm, $\epsilon_1 = 9.6$, $W/H_1 = 1.57$).

Fig. 9(a). The configuration of the first example for right-angle bends is used with a W/H ratio of 2. The S parameters are compared for a compensation ratio of $s/W = 0.83$. Fig. 9(a) shows the magnitude of S_{11}. For the compensated case a considerable reduction of S_{11} is achievable. The ratio of S_{11} for the compensated case and S_{11} for the uncompensated case is about 0.125 at the low frequency end at 6 GHz and 0.27 at the high frequency end at 20 GHz. Comparing the deviation in the phase of S_{11} (Fig. 9(b)) yields a change of capacitive to inductive loading, which is due to the increased current crowding effect in the corner region of the compensated edge.

V. Conclusion

An enhanced algorithm for the full-wave analysis of microstrip discontinuities on a double-layered substrate has been presented. The procedure is based on the use of index tables that are computed from 2-D discrete FFT routines. Elements of the associated moment matrix are then derived

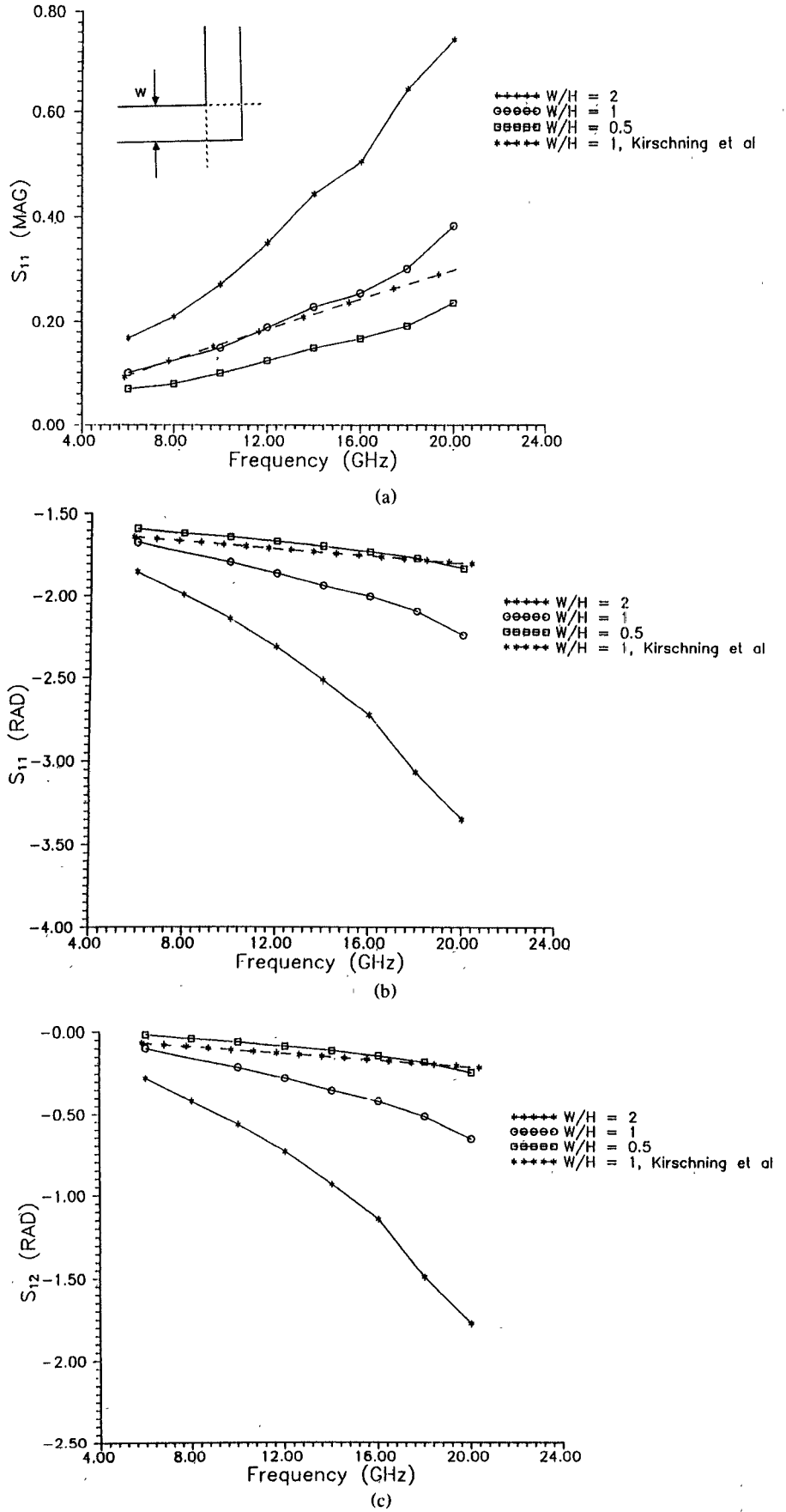

Fig. 6. S parameter of right-angle bend for various W/H_1 ratios ($a = b = 12.7$ mm, $c = 3.18$ mm, $H_1 = 0.635$ mm, $\epsilon_1 = 9.8$): (a) S_{11} (MAG); (b) S_{11} (RAD); (c) S_{12} (RAD). Dotted lines in the inset represent reference planes.

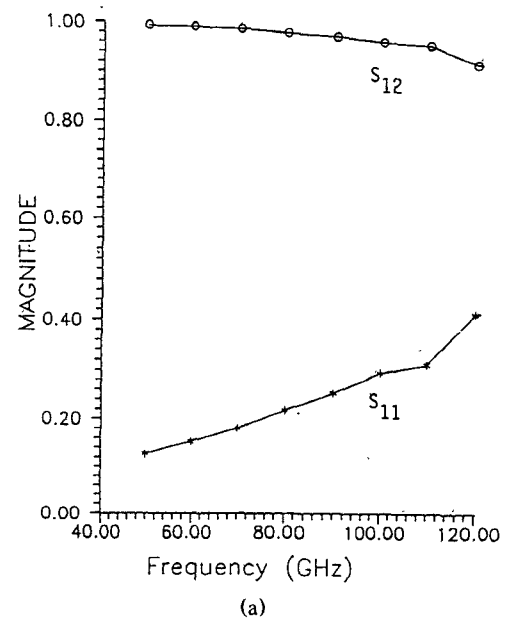

(a)

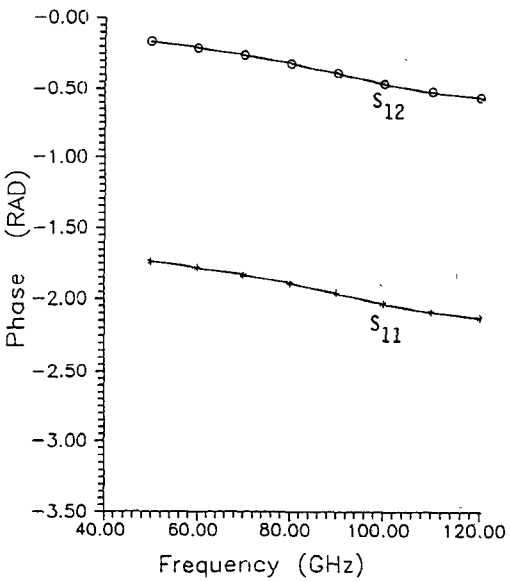

(b)

Fig. 7. S parameter of right-angle bend, double-layered substrate ($a = b = 1.9$ mm, $c = 1.05$ mm, $H_1 = 0.1$ mm, $H_2 = 0.005$ mm, $\epsilon_1 = 12.9$, $\epsilon_2 = 3.9$, $W = 0.1$ mm): (a) S_{11} (MAG), S_{12} (MAG); (b) S_{11} (RAD), S_{12} (RAD).

from a simple linear combination of the elements in the index table. The method was applied to simulate resonant modes for various discontinuity structures, including the effect of the shielding walls, in order to demonstrate its capabilities. The presented technique should be helpful in the characterization of single and coupled microstrip discontinuities for (M)MICs.

Acknowledgment

The authors gratefully acknowledge the helpful correspondence and discussions with Dr. N. H. L. Koster of Duisburg University, Federal Republic of Germany, and A. Skirevik of Ecole Polytechnique, Luasanne.

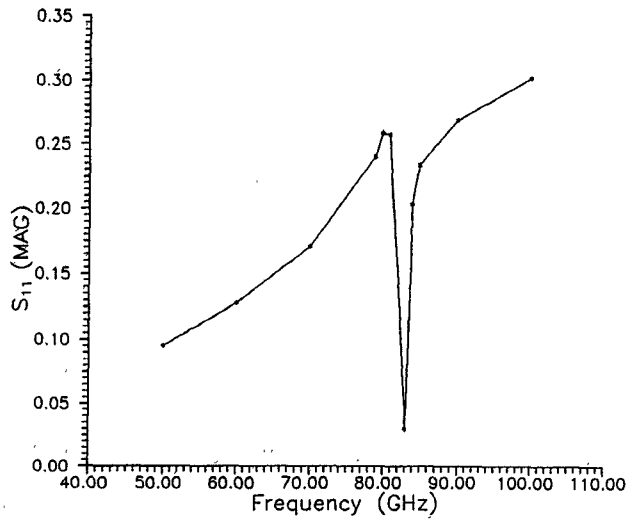

Fig. 8. S_{11} (MAG) of right-angle bend at box resonances $a = b = 1.9$ mm, $c = 0.2$ mm, $H_1 = 0.1$ mm, $W/H_1 = 1$).

Appendix

Expressions for the components of the Green's dyadic in (1) are summarized. Define

$$Umn = 1 - \frac{\epsilon_2}{\epsilon_1}\frac{T_{mn1}T_{mn2}}{k_{zmn2}^2} + \left(\frac{T_{mn1}}{\epsilon_1} + \frac{T_{mn2}}{\epsilon_2}\right)\frac{\epsilon_3}{T_{mn3}} \tag{A1}$$

$$V_{mn} = 1 - \frac{T_{mn1}T_{mn2}}{k_{zmn1}^2} + \left(\frac{T_{mn1}}{k_{zmn1}^2} + \frac{T_{mn2}}{k_{zmn2}^2}\right)\frac{k_{zmn3}^2}{T_{mn3}} \tag{A2}$$

$$X_{mn} = \frac{R_{mn}}{(k_{xmn}^2 + k_{ymn}^2)U_{mn}} \tag{A3}$$

$$Y_{mn} = \frac{S_{mn}}{(k_{xmn}^2 + k_{ymn}^2)V_{mn}} \tag{A4}$$

$$Z_{mn} = X_{mn} - Y_{mn} \tag{A5}$$

$$R_{mn} = \frac{T_{mn1}}{\epsilon_1} + \frac{T_{mn2}}{\epsilon_2} \tag{A6}$$

$$S_{mn} = k_0^2\left(\frac{T_{mn1}}{k_{zmn1}^2} + \frac{T_{mn2}}{k_{zmn2}^2}\right) \tag{A7}$$

$$F_{mn} = L_{mn}\frac{j\omega\epsilon_0}{ab} \tag{A8}$$

$$L_{mn} = \begin{cases} 4, & m \text{ and } n > 0 \\ 0, & m \text{ and } n = 0 \\ 2, & m \neq 0 \text{ and } n = 0 \text{ or } n \neq 0 \text{ and } m = 0 \end{cases} \tag{A9}$$

$$k_0^2 = \frac{\omega^2}{v^2} \tag{A10}$$

$$k_{xm} = \frac{m\pi}{a} \qquad k_{yn} = \frac{n\pi}{b} \tag{A11}$$

$$k_{zmni} = \sqrt{k_0^2\epsilon_i - (k_{xm}^2 + k_{yn}^2)} \tag{A12}$$

$$T_{mni} = k_{zmni}\tan(k_{zmni}H_i). \tag{A13}$$

Then,

$$XY_{mn} = k_{xm}^2 X_{mn} + k_{yn}^2 Y_{mn} \tag{A14}$$

$$YX_{mn} = k_{yn}^2 X_{mn} + k_{xm}^2 Y_{mn} \tag{A15}$$

$$RZ_{mn} = k_{xm}k_{yn}Z_{mn}. \tag{A16}$$

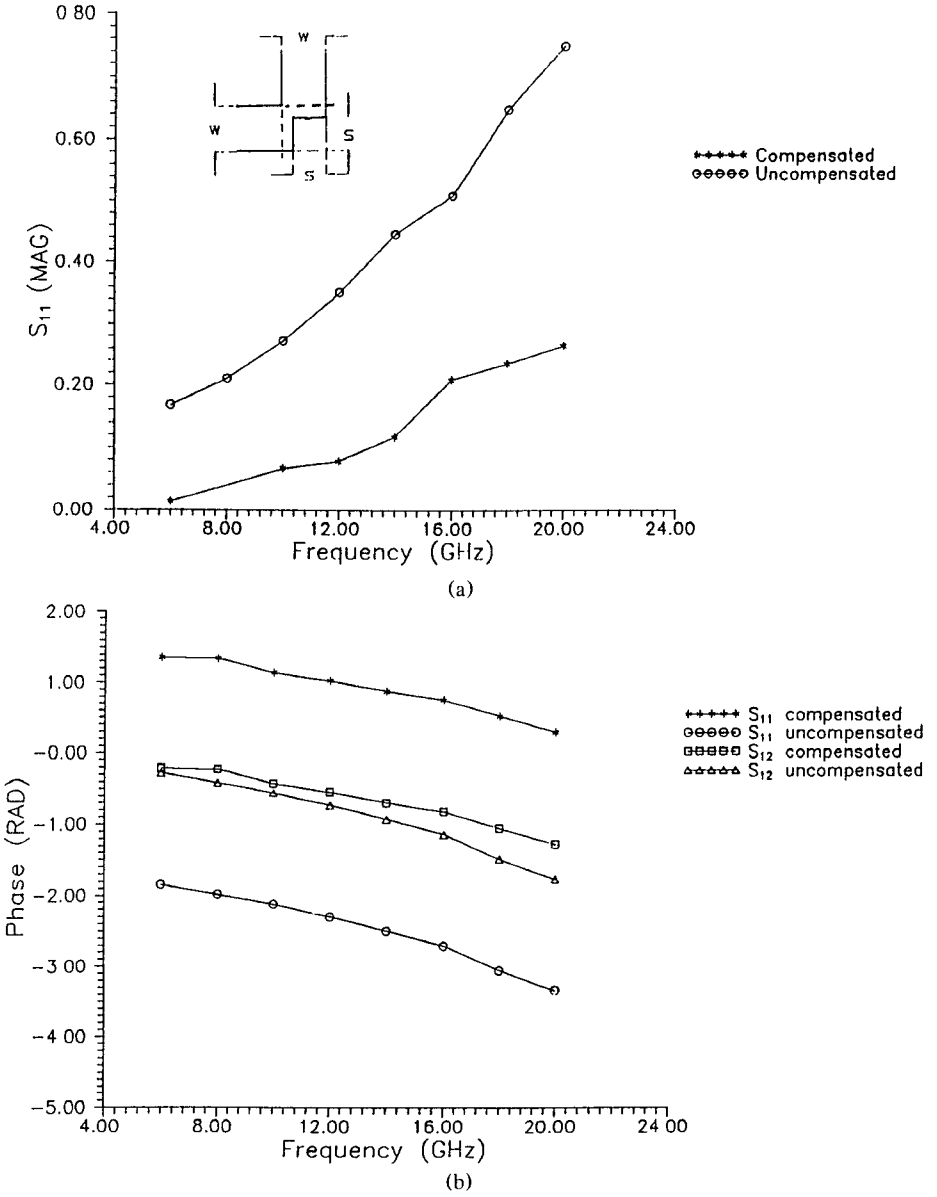

Fig. 9. Comparison of S parameter for compensated bend and right-angle bend ($a = b = 12.7$ mm, $c = 3.18$ mm, $H_1 = 0.635$ mm, $\epsilon_1 = 9.8$, $W/H_1 = 2$): (a) S_{11} (MAG); (b) S_{11} (RAD), S_{12} (RAD). Dotted lines in the inset represent reference planes.

References

[1] T. Itoh, Ed., *Numerical Techniques for Microwave and Millimeter Wave Passive Structures*. New York: Wiley, 1989.

[2] I. Wolff *et al.*, "Calculation method for microstrip discontinuities and T-junctions," *Electron. Lett.*, vol. 8, pp. 177–179, 1972.

[3] T. S. Chu and T. Itoh, "Analysis of microstrip discontinuity by the modified residue calculus technique," *IEEE Trans. Microwave Theory Tech.*, vol. MTT-33, pp. 1024–1028, Oct. 1985.

[4] N. H. L. Koster and R. H. Jansen, "The microstrip step discontinuity: A revised description," *IEEE Trans. Microwave Theory Tech.*, vol. MTT-34, pp. 213–222, Feb. 1986.

[5] P. B. Katehi and N. G. Alexopoulos, "Frequency-dependent characteristics of microstrip discontinuities in millimeter-wave integrated circuits," *IEEE Trans. Microwave Theory Tech.*, vol. MTT-33, pp. 1029–1035, Oct. 1985.

[6] R. W. Jackson and D. M. Pozar, "Full-wave analysis of microstrip open-end and gap discontinuity," *IEEE Trans. Microwave Theory Tech.*, vol. MTT-33, pp. 1036–1042, Oct. 1985.

[7] R. H. Jansen, "Hybrid mode analysis of end effects of planar microwave and millimetrewave transmission lines," *Proc. Inst. Elec. Eng.*, vol. 128, pt. H, no. 2, pp. 77–86, Apr. 1981.

[8] N. H. L. Koster, "Zur charakterisierung der frequenzabhaengigen Eigenschaften von Diskontinuitaeten in planaren Wellenleitern," Ph.D. thesis, Universitaet Duisburg, 1984.

[9] R. Sorrentino and T. Itoh, "Transverse resonance analysis of finline discontinuities," *IEEE Trans. Microwave Theory Tech.*, vol. MTT-32, pp. 1633–1638, December 1984.

[10] L. P. Schmidt, "Zur feldtheoretischen Berechnung fon transversalen Diskontinuitaeten in Mikrostrip-Leitungen," Ph.D. thesis, RWTH Aachen, West Germany, 1979.

[11] W. L. Chang, "Filterelemente and Resonatoren aus geschirmten Streifenleitungen mit sprunghafter Breitenaenderung," Ph.D. thesis, TH Darmstadt, West Germany, 1977.

[12] J. C. Rautio, "A time-harmonic electromagnetic analysis of shielded microstrip circuits," Ph.D. thesis, Syracuse University, Syracuse, NY, 1986.

[13] J. C. Rautio and R. F. Harrington, "An electromagnetic time-harmonic analysis of shielded microstrip circuits," *IEEE Trans. Microwave Theory Tech.*, vol. MTT-35, pp. 726–730, Aug. 1987.

[14] R. H. Jansen, "The spectral-domain approach for microwave integrated circuits," *IEEE Trans. Microwave Theory Tech.*, vol. MTT-33, pp. 1043–1056, Oct. 1985.
[15] A. W. Glisson and D. R. Wilton, "Simple and efficient numerical methods for problems of electromagnetic radiation and scattering from surfaces," *IEEE Trans. on Antennas and Propagation*, vol. AP-28, pp. 593–603, September 1980.
[16] R. W. Jackson, "Full-wave, finite element analysis of irregular microstrip discontinuities," *IEEE Trans. Microwave Theory Tech.*, vol. 37, pp. 81–89, Jan. 1989.
[17] A. Skrivervik and J. R. Mosig, "Equivalent circuits of microstrip discontinuities including radiation effects," in *IEEE MTT-S Int. Microwave Sump. Dig.*, 1989, pp. 1147–1150.
[18] Z. J. Cendes and J. Lee, "The transfinite element method for modeling MMIC devices," *IEEE Trans. Microwave Theory Tech.*, vol. 36, pp. 1639–1649, Dec. 1988.
[19] W. P. Harokopus and P. B. Katehi, "An accurate characterization of open microstrip discontinuity including radiation losses, in *IEEE MTT-S Int. Microwave Symp. Dig.*, 1989, pp. 231–234.
[20] B. S. Worm and R. Pregla, "Hybrid-mode analysis of arbitrarily shaped planar microwave structures by the method of lines, *IEEE Trans. Microwave Theory Tech.*, vol. MTT-32, pp. 191–196, Feb. 1984.
[21] J. R. Mosig, "Arbitrarily shaped microstrip structures and their analysis with a mixed potential integral equation," *IEEE Trans. Microwave Theory Tech.*, vol. 36, pp. 314–323, Feb. 1988.
[22] Z. Chen and B. Gao, "Deterministic approach to full-wave analysis of discontinuities in MICs using the method of lines," *IEEE Trans. Microwave Theory Tech.*, vol. 37, pp. 606–611, Mar. 1989.
[23] A. Nakatani, S. A. Maas, and J. Castaneda, "Modeling of high frequency MMIC passive components," in *IEEE MTT-S Int. Microwave Symp. Dig.*, 1989, pp. 1139–1142.
[24] W. Wertgen and R. H. Jansen, "Spectral iterative techniques for the full-wave 3D analysis of (M)MIC structures," in *IEEE MTT-S Int. Microwave Symp. Dig.*, 1988, pp. 709–712.
[25] R. J. Jansen and L. Wiemer, "Full-wave theory based development of mm-wave circuit models for microstrip open end, gap, step, bend and tee," in *IEEE MTT-S Int. Microwave Symp. Dig.*, 1989, pp. 779–782.
[26] L. P. Dunleavy and P. B. Katehi, "A generalized method for analyzing shielded thin microstrip discontinuities," *IEEE Trans. Microwave Theory Tech.*, vol. 36, pp. 1758–1766, Dec. 1988.
[27] L. P. Dunleavy and P. B. Katehi, "Shielding effects in microstrip discontinuities," *IEEE Trans. Microwave Theory Tech.*, vol. 36, pp. 1767–1774, Dec. 1988.
[28] L. P. Dunleavy, "Discontinuity characterization in shielded microstrip: A theoretical and experimental study," Ph.D. thesis, University of Michigan, 1988.
[29] R. H. Jansen and N. H. L. Koster, "Accurate results on the end effect of single and coupled lines for use in microwave circuit design," *Arch. Elek. Übertragung.*, Band 34, pp. 453–459, 1980.
[30] M. Kirschning *et al.*, "Measurement and computer aided modelling of microstrip discontinuities by an improved resonator method," in *IEEE MTT-S Int. Microwave Symp. Dig.*, 1983, pp. 495–497.
[31] R. R. Jansen and W. Wertgen, "Modular source-type 3D analysis of scattering parameters for general discontinuities, components and coupling effects in (M)MIC's," in *Proc. 17th European Microwave Conf.* (Rome), Sept. 1987, pp. 427–437.
[32] A. Hill, "Quasi-TEM and full wave numerical methods for the characterization of microstrip discontinuities," Ph.D. thesis, Oregon State University, Corvallis, OR, 1989.

Achim Hill was born in Friedrichshafen, West Germany, on October 28, 1960. He received the Dipl-Ing. degree in physical electronics from the University of Stuttgart, Germany, where he studied from 1981 to 1985. During the academic year 1985–1986 he was a Fulbright scholar in the Electrical and Computer Engineering Department at Oregon State University. He received the M.S. and Ph.D. degrees in electrical engineering from Oregon State University, Corvallis, in 1986 and 1989 respectively. During part of his studies he was a tutor and research assistant and a scholar of the Friedrich-Ebert Studienstiftung.

He recently joined Compact Software Inc., Paterson, NJ, where he is responsible for electromagnetic simulations of microwave and millimeter-wave passive components.

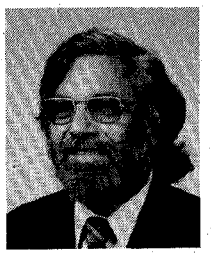

Vijai K. Tripathi (M'68–SM'87) received the B.Sc. degree from Agra University, Uttar Pradesh, India, in 1958, the M.Sc. Tech. degree in electronics and radio engineering from Allahabad University, Uttar Pradesh, India, in 1961, and the M.S.E.E. and Ph.D. degrees in electrical engineering from the University of Michigan, Ann Arbor, in 1964 and 1968, respectively.

From 1961 to 1963, he was a Senior Research Assistant at the Indian Institute of Technology, Bombay, India. In 1963, he joined the Electron Physics Laboratory of the University of Michigan, where he worked as a Research Assistant from 1963 to 1965 and as a Research Associate from 1966 to 1967 on microwave tubes and microwave solid-state devices. From 1968 to 1973, he was an assistant Professor of Electrical Engineering at the University of Oklahoma, Norman. In 1974, he joined Oregon State University, Corvallis, where he is a Professor of Electrical and Computer Engineering. His visiting and sabbatical appointments have included the Division of Network Theory at Chalmers University of Technology in Gothenburg, Sweden, from November 1981 through May 1982; Duisburg University, Duisburg, Germany, from June through September 1982; and the Electronics Technology Division of the Naval Research Laboratory in Washington, DC, in the summer of 1984. His current research activities are in the areas of microwave circuits and devices, electromagnetic fields, and solid-state devices.

Dr. Tripathi is a member of Eta Kappa Nu and Sigma Xi.